Journal of Alloys and Compounds 745 (2018) 569–578

Contents lists available at ScienceDirect

Journal of Alloys and Compounds

journal homepage: http://www.elsevier.com/locate/jalcom

Effect of ablative angles on the ablation behaviors of ZrB_2-SiC modified carbon/carbon composites

Chuang Wang [a, b], Ke-zhi Li [b, *], Ying Lu [b], Lei Peng [a], Bingliang Li [a], Zhigang Zhao [b]

[a] Shaanxi Province Engineering Laboratory of High Performance Concrete, Shaanxi Railway Institute, Weinan 714099, PR China
[b] School of Materials Science and Engineering, Northwestern Polytechnical University, Xi'an 710072, PR China

ARTICLE INFO

Article history:
Received 2 December 2017
Received in revised form
20 January 2018
Accepted 18 February 2018
Available online 22 February 2018

Keywords:
Carbon/carbon
Ceramic-matrix composites
Ablative angle
Morphology

ABSTRACT

To analyze the effect of different ablation angles on the ablative property of carbon/carbon(C/C) composites modified by ZrB_2-SiC, C/C-ZrB_2-SiC composites (ZS) were prepared via precursor infiltration and pyrolysis (PIP). The prepared composites (ZS) were then ablated by oxyacetylene flame at 90° and 0° angles (ZS-90° and ZS-0°), respectively. The results show that, at ZS-0° angle, the ablation resistance was worse due to the existence of turbulent flame. The temperature in the inner cone and the gas flow velocity at ZS-0° were higher than those at ZS-90°. At ZS-90°, the damage of the composites was dominated by the thermo-chemical ablation. The ablation mechanism at ZS-0° was mainly the mechanical denudation with the thermo-chemical ablation as supplement. The dissimilar ablation angles of the C/C-ZrB_2-SiC composites under the oxyacetylene flame resulted in the distinct ablation resistance on the surfaces, hence different ablation mechanisms.

1. Introduction

Carbon/carbon (C/C) composites is one of the most promising candidate materials for various high-temperature application components. It has been used as nose tips, leading edges, heat shields, nozzles of a solid rocket motor and other thermal protection systems for space vehicles [1–4] due to its unique properties, such as high strength-to-weight ratio, high thermal conductivity and good thermal shock resistance. However, the poor oxidization and ablation resistance properties of the C/C composites under ultrahigh temperature and high pressure heat flux environments have seriously limited its applications in advanced aerospace fields. Up to now, great efforts have been made to elevate its oxidation [5–7] and ablation [8,9] resistance properties so as to adapt to the more advanced space systems or other much more rigorous service conditions.

Ultrahigh temperature ceramics are usually refractory carbide/boride compounds. When they are introduced into the C/C composite matrix, they can be used as an effective solution to improve the ablation resistance of the C/C composites [10–14]. Among them, ZrB_2 has attracted much attention for its special properties: very high melting temperature (3243 °C), good thermal shock resistance, and good chemical inertness [15]. Its oxidized product ZrO_2 also has a high melting point (in excess of 2600 °C), which is helpful for improving the ablation resistance by reducing the oxygen diffusion rate into the inner C/C matrix [16]. Additionally, it has been widely reported that the addition of SiC into the C/C matrix can improve the anti-oxidation and ablation property of pure ultrahigh temperature ceramics effectively because of the formation of less volatile silica-containing scales [11,17,18]. Therefore, a well-designed ZrB_2-SiC modified C/C composites can offer a reliable anti-ablation property for a long term in ultrahigh temperatures.

So far, many researchers have prepared C/C-ZrB_2-SiC composites via different precursor infiltration and pyrolysis (PIP) methods. By these methods, isolated and coupled ZrB_2-SiC particles are introduced into the C/C matrix to investigate the effect of phase distribution on the ablation behavior [12]. Some researches are mainly focused on the influence of ceramic additives content, heat flux and ablation time on the ablation performance of the as-prepared composites. The oxyacetylene flame ablation, laser ablation [19,20], arc stagnation ablation and wind tunnel test are applied to discuss the anti-ablation property of C/C-ZrB_2-SiC composites. However, in the practical service environment, the shape of a component is diverse, the temperature is unstable, and the gas flow changes, so the angles between the gas flow and the component are always diverse and vary from time to time. Unfortunately, the

* Corresponding author. Tel.: +86 2221125x0913.
E-mail address: likezhi@nwpu.edu.cn (K.-z. Li).

https://doi.org/10.1016/j.jallcom.2018.02.228
0925-8388/

influence of different ablative angles on the ablation resistance has been seldom reported so far yet, which has greatly constrained the further application of the C/C-ZrB_2-SiC composites.

With this in mind, in the present work, the C/C-ZrB_2-SiC composites (ZS) was prepared by a precursor infiltration and pyrolysis (PIP) method. The thermal physical properties of the prepared ZS composites were measured with Archimedes method. The ablation behaviors were tested in an oxyacetylene torch under two ablation angles 90° and 0° (hereinafter referred to as ZS-90° and ZS-0°), respectively. The phase and composition of the composites before and after ablation were identified by X-ray diffraction. The microstructure and morphologies were observed and analyzed by scanning electron microscopy (SEM) equipped with energy dispersive spectroscopy (EDS). The fundamental ablation mechanism was proposed correspondingly.

2. Experimental

2.1. Preparation of the C/C-ZrB_2-SiC composites

The schematic preparation procedures of the C/C-ZrB_2-SiC composites are shown in Fig. 1. As can be seen from the flow chart, 2.5D needle punched carbon felts (0.45 g/cm^3) was firstly densified through thermal gradient chemical vapor infiltration (TCVI) for 20–50 h between 900 °C and 1100 °C. Natural gas was used as a carbon precursor. The porous C/C composites were then fabricated after being graphitized between 2300 °C and 2500 °C under the protection of Ar gas. Finally, ZrB_2 and SiC were introduced into the preform by the precursor infiltration and pyrolysis process.

ZrB_2 polymeric precursor (Institute of Process Engineering, Chinese Academy of Sciences; Ceramic productivity was approximately 30 wt%) and polycarbosilane (PCS, the National University of Defense Technology; Ceramic productivity was approximately 55 wt%) were mixed with a weight ratio of 2:1 to form a homogenous solution, using dimethylbenshix as a solvent. After the preform was immersed into the as-prepared solution under vacuum for 0.5 h, the samples were taken out and dried at 90 °C for 24 h. They were then heat treated at 1500 °C for 2 h in a flowing Ar atmosphere in order to convert the precursor into ZrB_2 and SiC particles. The precursor infiltration and pyrolysis process was repeated for many cycles until the final weight gain was less than 2%. Eventually, the C/C-ZrB_2-SiC composites with an apparent density approximately 1.80 g/cm^3 was prepared.

2.2. Measurement of the thermal physical properties

The density and open porosity of the C/C-ZrB_2-SiC samples were measured with Archimedes method. According to GJB1201.1–1991, the thermal diffusivity and specific heat capacity of the composites were measured using a TC-3000 thermal properties analyzer. The test directions were perpendicular to the carbon felts (the needled direction) and parallel to it. The sample dimension was Ø12.6 × 3 mm. The thermal conductivity of the sample was calculated by Eq. (1).

$$\lambda = \alpha \times Cp \times \rho \quad (1)$$

where α is the thermal diffusivity, C_p is the specific heat capacity at constant pressure, and$\rho$is the density of the composites.

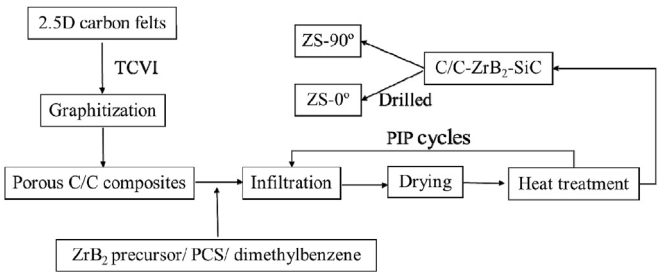

Fig. 1. Schematic preparation procedure of the C/C-ZrB_2-SiC composites.

2.3. Ablation test

The ablation tests were carried out in the oxyacetylene torch in accordance with GJB322A-96. The ablation parameters are shown in Table 1. The inner diameter of the nozzle tip was 2 mm and the distance between it and the sample was 10 mm. The samples, with the dimension of Ø30 × 10 mm, were cut from the prepared C/C-ZrB_2-SiC composites and abraded by 400 grit SiC paper. In the meanwhile, a hole with the diameter of 5 mm was drilled in the center of some samples as shown in Fig. 2(a). The ablation gun was primarily ignited. As the flame was stable, the sample was vertically placed to the flame as shown in Fig. 2(b). Thus, the ablation angles can be ensured at 0° as shown in Fig.(2)c and 90° as shown in Fig. 2(d) where the inner cone of the oxyacetylene flame can go through the hole exactly.

2.4. Characterization

An infrared thermometer (Raytek MR1SCSF) in 2-color mode with an error of ±0.75% was used to measure the temperature of the center surface and the entrance hole of the C/C-ZrB_2-SiC composites at 90° and 0°, respectively. The mass and linear ablation rates were calculated according to the following equations (2) and (3). The average value of three samples was taken as the ultimate data.

$$Rm = \frac{m0 - m1}{t} \quad (2)$$

$$Rl = \frac{d0 - d1}{t} \quad (3)$$

where R_m and R_l are mass and linear ablation rates; m is the mass of the sample; d is the thickness of ZS-90° at the ablation center or the hole diameter of ZS-0°; t is the ablation time and it is 120 s in this experiment. The subscripts "0" and "1" represent parameters before and after ablation, respectively.

The phase and the composition of the sample before and after ablation were identified by X-ray diffraction (XRD, X'Pert Pro MPD). The microstructure and morphologies of ZS-90° and ZS-0° were observed and analyzed by scanning electron microscope (SEM, TESCAN VEGA3) equipped with energy dispersive spectroscopy (EDS).

Table 1
Ablation parameters of the oxyacetylene torch.

Flux (L/s)		Pressure (MPa)		Heat flux (MW/m^2)	Ablation angle (°)
O_2	C_2H_2	O_2	C_2H_2		
0.42	0.31	0.4	0.095	4.2	90 and 0

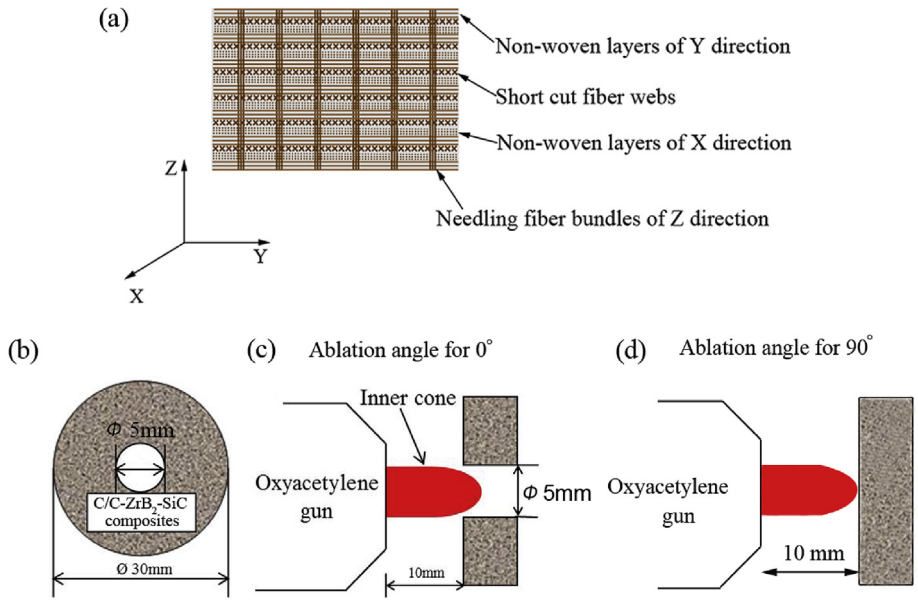

Fig. 2. The structure illustration of the C/C-ZrB_2-SiC composites under an oxyacetylene flame: (a) The X, Y, and Z coordinate system to show directions; (b) The sample with a hole diameter of 5 mm; (c) Ablation angle for 0°; (d) Ablation angle for 90°.

3. Results and discussion

3.1. Microstructure and phase characterization of the C/C-ZrB_2-SiC composites

Fig. 3 shows the back-scattered electron images (BSE) morphology of the internal surface of ZS-0° before ablation, which is similar to that cross-sectional morphology of ZS-90°. From the EDS analysis in the inset in Fig. 3(b), it can be seen that the samples contain elements of Si, Zr, B, C, and O, of which Si, Zr, and B are dominant. To find out the composition of the composites, XRD pattern are shown in Fig. 4 from which it can be seen that the composites are mainly composed of ZrB_2 and SiC in addition to a little amount of ZrC and C, indicating that the precursor was converted into ZrB_2 and SiC after heat treatment. These ceramic particles, which were formed during the precursor infiltration and pyrolysis process, were mainly concentrated in short-cut webs between two non-woven webs as shown in Fig. 3(a). As a result of the high SiC ceramic yield (55 wt%), the gray SiC can combine with white ZrB_2 to form a whole. The lower thermal expansion coefficient of SiC can reduce the mismatch between the carbon matrix and ZrB_2 particles, which is advantageous to the application of C/C-ZrB_2-SiC composites at high temperature [21].

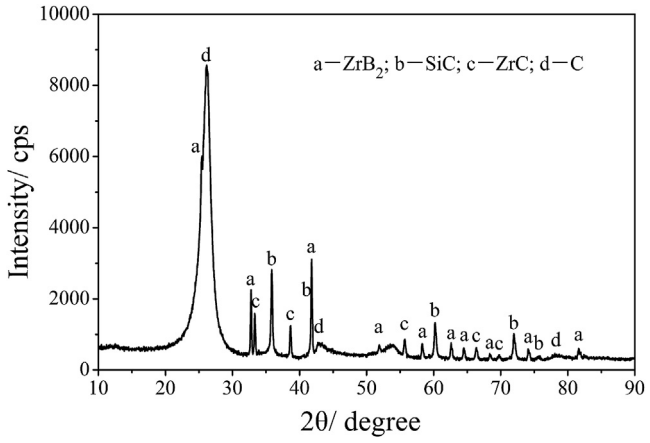

Fig. 4. XRD pattern of the prepared C/C-ZrB_2-SiC composites.

No large closed-pores were observed, which indicates that the infiltration solution had strong penetration ability. The existence of

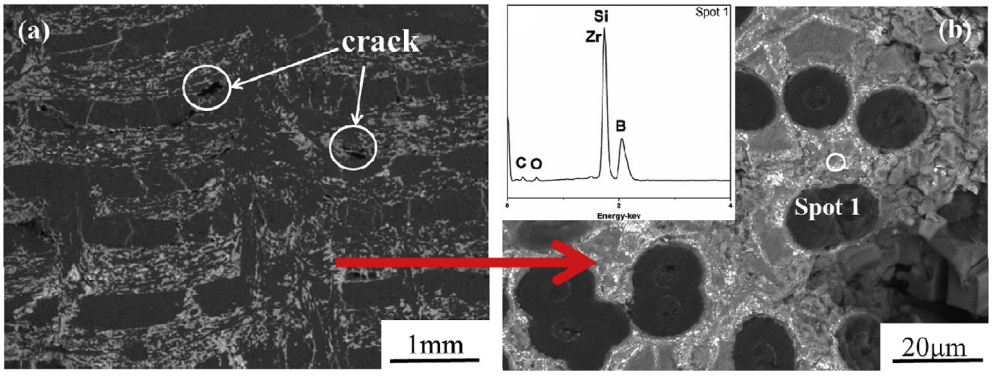

Fig. 3. BSE morphology and EDS analysis of internal surface of ZS-0° before ablation: (a) at low magnification; (b) at high magnification.

preferential infiltration can contribute to the non-uniform distribution of ceramic particles, as the pores in short-cut webs were much bigger than those in the non-woven webs. However, more discernible cracks in the interface could be observed in ZS-0°, as the curved internal surface is more difficult to process than the plane one of ZS-90°. In addition, the inherent hard and brickle characters of ZrB_2 and SiC ceramic particles make the brittle failures easily occur during the machining process, finally resulting in the ceramic bulk peeling off the interface of ZS-0°.

3.2. Ablation properties of the C/C-ZrB_2-SiC composites

The surface temperatures of both ZS-0° and ZS-90° samples were increased rapidly to the maximum values, i.e. 2260 °C and 2300 °C, and then remained constant at a relatively stable level as shown in Fig. 5. The temperature fluctuation of ZS-0° was larger and its maximum value was up to 2300 °C, while the maximum temperature of ZS-90° was 2260 °C. The temperatures of both ZS-0° and ZS-90° samples reached the same plateau at the end of this process.

On the one hand, due to the existence of a hole in ZS-0°, the inner cone went through the entrance at a sharp angle according to Fig. 2(b). The transition of the flame was not very gentle when it ran into a narrow space in a sudden. It was more likely to form turbulent flame at the entrance hole, in which the temperature is higher and the air velocity is faster than in the laminar flame that was formed during the ablation of ZS-90° [22]. Therefore, it was believed that the Tmax of ZS-0° is higher than that of ZS-90°.

On the other hand, the thermal constants of the C/C-ZrB_2-SiC composites were different at different directions as shown in Fig. 6. As can be seen from the figure, the thermal diffusion in Fig. 6(a), the specific heat capacity in Fig. 6(b), and the thermal conductivity in Fig. 6(c) along the z direction were all higher than those along the xy direction because of the structural differentiation. At the z direction, the C/C-ZrB_2-SiC composites was connected by long fibers in non-woven webs, while it was stacked up by short-cut webs and non-woven webs alternately from top to bottom at the xy direction [23]. As a result, long fibers can serve as a smooth channel for the rapid heat transfer. However, most of the ceramic particles distributed in the short-cut webs along with numerous holes and cracks became obstructions during the heat transfer process. That is to say, the corresponding ZS-0° ablation samples own a higher heat transfer rate than ZS-90°.

Consequently, the heat transferred onto the surface of ZS-0° can spread to the surroundings more quickly, thus reducing the heat accumulation during ablation process. Meanwhile, the heat flux that mainly concentrated on the inner cone can run away to the ambient atmosphere through the hole of ZS-0°. This may result in a lower Tmax. These few opposite effects explained above will play dominant or secondary roles during different ablation processes. The results were in accord with the experimental data.

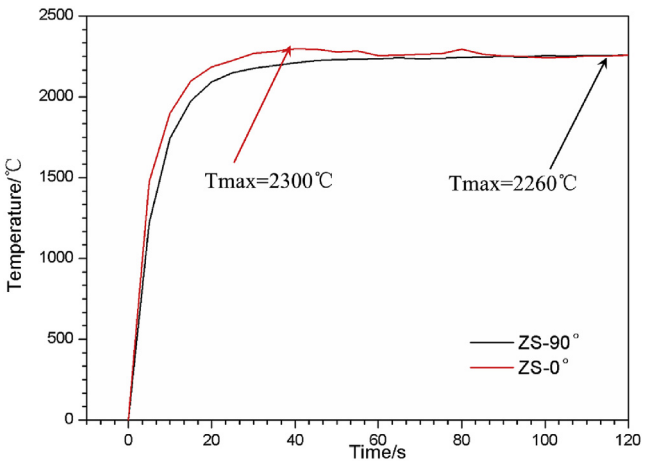

Fig. 5. Surface temperature curves of both the ablation center of ZS-90° and the entrance hole of ZS-0°.

The mass ablation rates of ZS-90° and ZS-0° are 2.075×10^{-4} g/s and 5.940×10^{-4} g/s, respectively. The liner ablation rate of ZS-90° is 1.3×10^{-3} mm/s. As to ZS-0°, the diameter of the hole was reduced with the increasing of the distance to the entrance and some parts of the hole were even smaller than the original size (5 mm). Consequently, it corresponds to a negative liner ablation rate in these parts as shown in Fig. 7(b). It can also be inferred that the erosion at different parts in the hole was various.

The macro-morphologies of C/C-ZrB_2-SiC composites after ablation for 120 s at different angles are shown in Figs. 7(a) and Fig. 8(a). Along the direction of oxyacetylene flame, the internal surface of ZS-0° as observed in Fig. 7(a) displays three different morphologies: the entrance ablation region, the transition region, and the tail region, which are represented by capital letters A, B, and C, respectively. While for ZS-90° as shown in subsequent Fig. 8(a), the ablated surface can also be divided into three concentric rings on the basis of appearance differences: the center ablation region, the transition region, and the brim region, which are represented by capital letters C, T, and B, respectively. In Fig. 8(d), the EDS curve shows the major elements are Si and O, while in Fig. 8(f), the EDS analysis shows the major elements are Zr and O.

3.3. Ablation morphologies

3.3.1. Ablation morphologies of ZS-90°

As shown in Fig. 8 above, the SEM images and the EDS spectrum of the center ablation region of ZS-90° were clearly observed. By further observation, it can be found that the surface of ZS-90° was covered with remnant composites, pits and ablation oxides as observed in Fig. 8(b). While more and more carbon fibers were naked with ablation time lengthening, some obvious grooves and ablated pits caused by denudation can easily be observed. The original morphologies of ZS-90° were already changed. Moreover, the residual ZrO_2 particles attached to the carbon fibers or sank into the grooves between fibers in the center-most region. It can be inferred from the phenomena that the ablation is mainly controlled by the mechanical erosion and oxidation.

Additionally, a discontinuous partially layered ZrO_2 structure with cracks existed near the center-most region as observed in Fig. 8(c). The cracks were mainly caused by the volume expansion of ZrO_2 because the drastic temperature changes after ablation would bring about the residual thermal stress and phase transition of ZrO_2. For one thing, the pores and cracks provide channels for oxidizing gas to further oxidize the underlying composites. In this case, new oxides will be generated and they can be acted as coatings to avoid further oxidation. For another, the newly generated oxides is conducive to the anti-ablation property for they can form a heat barrier on the surface of the composites when the gas diffuses out from the oxidation of C, SiC and ZrB_2.

It is well known that SiC is consumed faster than pyrocarbon and it loses its protection effect at high temperature over 2000 °C. Therefore, after ablation, ZrO_2 was generated as a result of oxidation of ZrB_2. But no peaks of SiO_2 were detected in the component of ZS-90° in the XRD pattern plotted in Fig. 9, from which it can be seen that, for ZS-0°, ZrO_2, C, ZrB_2, and SiO_2 were detected, but no ZrC was detected. For ZS-90°, ZrO_2, C, ZrB_2, and ZrC were detected, whereas no SiO_2 was detected. The reason is that most of SiO_2,

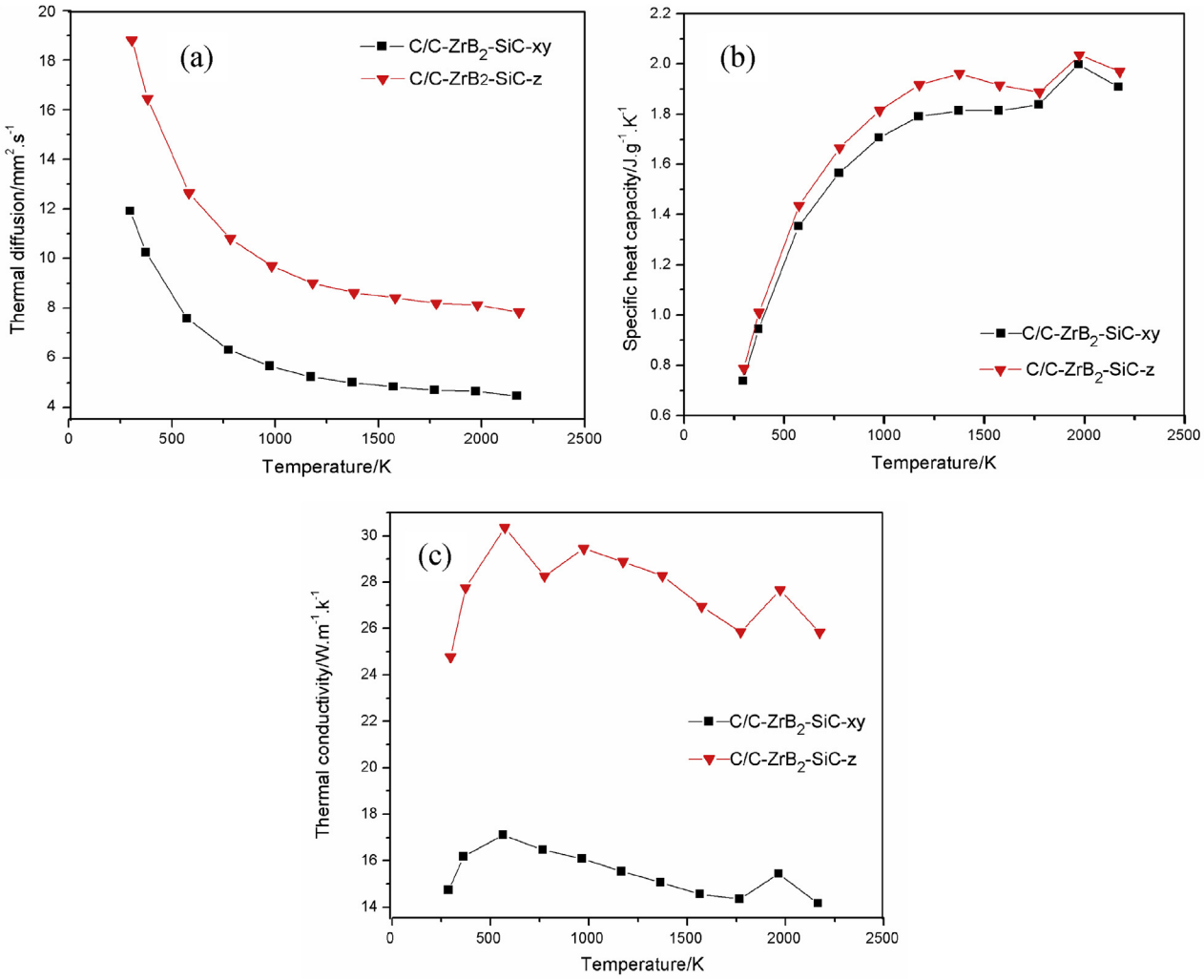

Fig. 6. The curves of thermal constants of C/C-ZrB_2-SiC composites (ZS) at different directions: (a) Thermal diffusion; (b) Specific heat capacity; (c) Thermal conductivity.

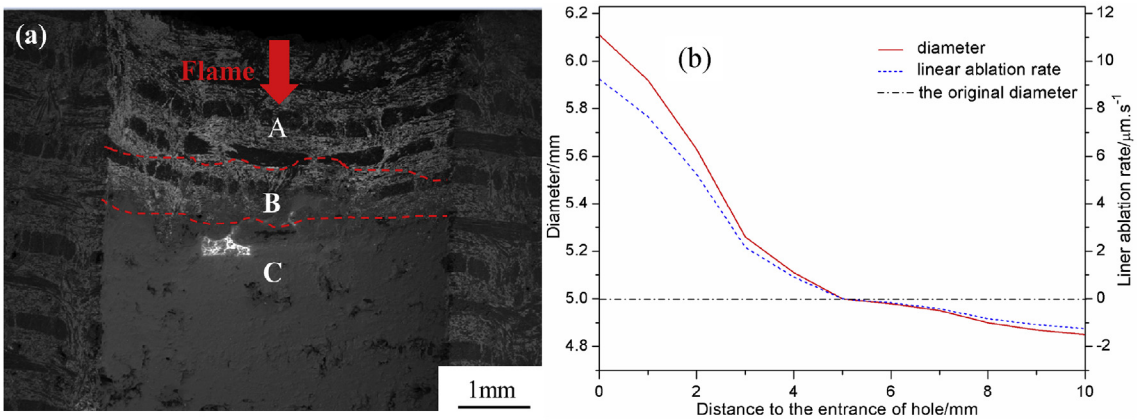

Fig. 7. The internal surface appearance of ZS-0° after ablation (split by half) (a) and the diameter of the internal hole versus the distance to the entrance of the hole (b). Capital letter A stands for the entrance ablation region, B refers to the transition region, and C means the tail region.

which was formed during ablation, was scoured away or evaporated. Therefore, its formation speed might be slower than the consumption speed. In addition, the surface temperature decreased sharply after the oxyacetylene torch was removed off from the sample, thus the residual SiO_2 was in a poor crystalline state. In this case, it was difficult to detect the existence of the residual SiO_2 [24]. It should be noted that the testing temperature at this region is almost 450 °C, much lower than the melting temperature of pure ZrO_2 (2700 °C). Consequently, the molten ZrO_2 is easily formed due to few SiO_2 existing in the solution, which can result in a lower

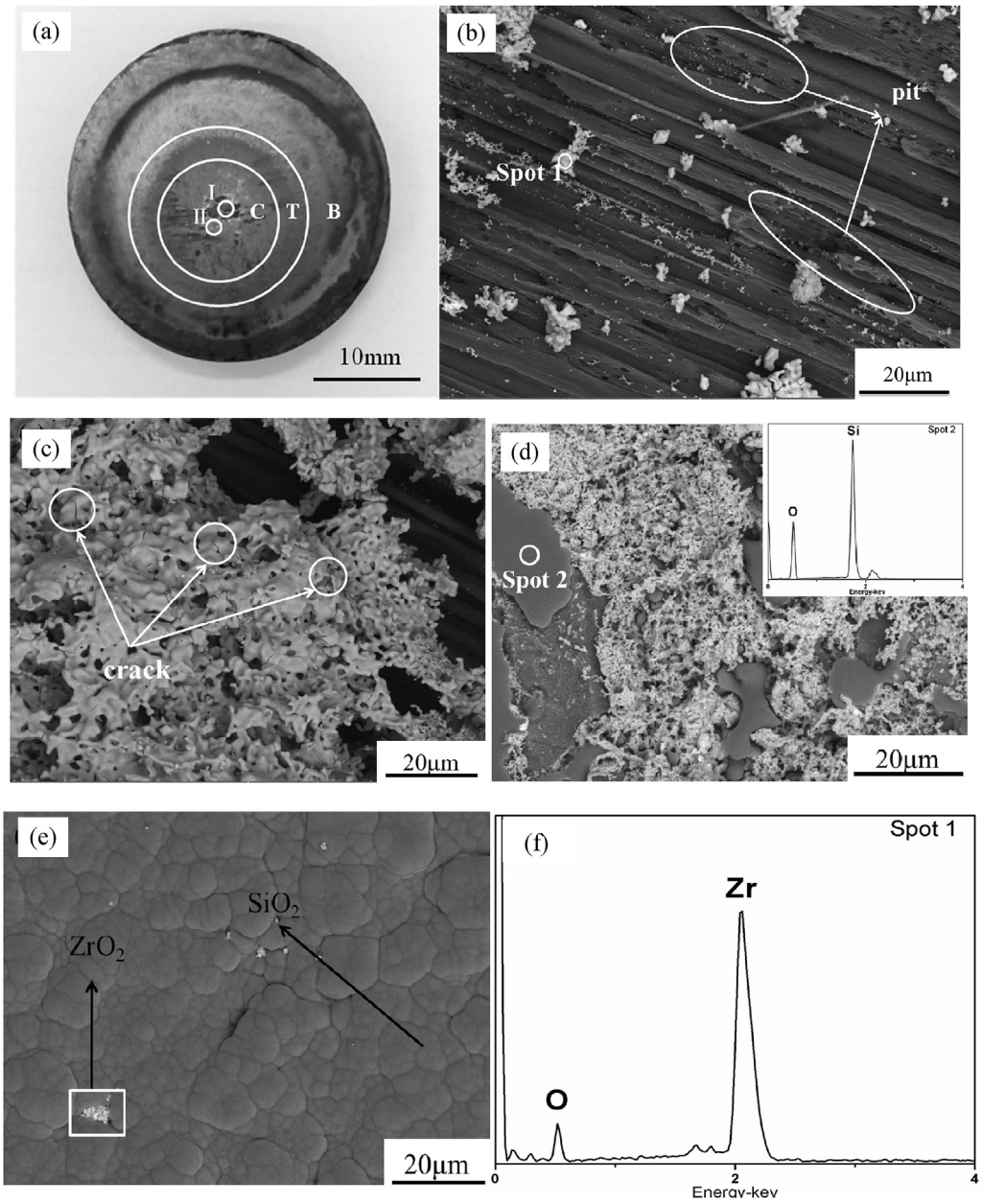

Fig. 8. (a) Digital images of ZS-90° after ablation; (b) and (c) high magnification of area I and II in (a); (d), (e) and (f) BSE morphology and EDS analysis in the transition and the brim region. Capital letters C, T, and B in (a) refer to the center ablation region, the transition region, and the brim region, respectively.

melting point of ZrO_2. As explained above, the protection of SiC was restricted, so the ablation resistance of the composites was mainly attributed to the molten ZrO_2. Structurally, ZrO_2 has rather high viscosity and strong adhesion to the composites. It is difficult for it to be blown away by the gas flow. Therefore, it can prevent the composites from further oxidation at ultrahigh temperature in this region.

Massive ZrO_2 particles can pack together to sprawl over the surface in the transitional region. Part of them was covered by a molten glassy SiO_2. A holding-on structure was formed as observed in Fig. 8(d). According to the corresponding EDS analysis, a dense gray glassy SiO_2 layer was covered on the brim ablation region. As shown in Fig. 8(e), a few of ZrO_2 was squeezed out as a result of the pressure change during the ablation and cooling processes. A structure was formed in which the SiO_2 outer layer coated on the holding-on ZrO_2-SiO_2 inner layer as measured by EDS in the inset in Fig. 8(d) and in Fig. 8(f) when associating with the morphology of the transitional region. But the interface between the two layers is blurry or transitional. Therefore, the ablation was dominated by the oxidation process. The formation of the SiO_2 layer was similar to the oxidation process of the ZrB_2-SiC composites [6]. As the dense SiO_2 layer possesses good viscosity and lower oxygen permeability rate, it can offer excellent anti-ablation protection for the modified composites. And it only produces a lower ablation mass in the brim region.

3.3.2. *Ablation morphologies of ZS-0°*

Fig. 10 shows the morphologies and relative EDS analysis of the entrance ablation region of ZS-0°. It can be observed in Fig. 10(a) that fibers perpendicular to the flame in the short-cut webs were

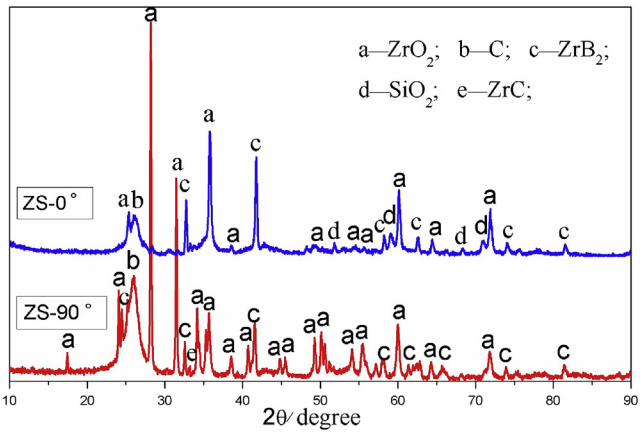

Fig. 9. XRD pattern of the C/C-ZrB_2-SiC composites after ablation.

ablated into sharp needle shapes and they located even lower than the pyrolytic carbon. This phenomenon was similar to that of carbon-based composites during oxidizing ablation or oxidation/sublimation process [25,26]. For carbon-based composites, sublimation can be neglected because the sublimation temperature of carbon/carbon composites at a standard atmospheric pressure is approximately 3727 °C and it increases with pressure [27]. Therefore, the formation of needle-shaped fibers was attributed to oxidation. The gaps between fibers and matrix can be clearly observed, which indicates that the fiber-matrix interface has weak ablation resistance and is apt to be oxidized. With the increasing of the heat flux, the viscosity of ZrO_2 was decreased. ZrO_2 was partially blown away to farther places in the hole. In addition to the coral-like clusters, some tiny spherical ZrO_2 was also found in the groove or adhere to fibers in the entrance area due to the continuous blowing of strong turbulent flame. According to Fig. 10(b), fibers perpendicular to the flame in the non-woven webs were ablated into flat-obtuse shapes. Fiber fractions were found in the left part according to the inset in Fig. 10(b) in which C, Si, and O are major elements.

Compared with the ZS-90° sample, the ZrO_2 layer in the ZS-0° sample seems to be at a more obvious molten state as observed in Fig. 10(c). Fig. 10(d) shows the corresponding EDS analysis from which it can be seen that the major elements are Si, Zr, C and O. Considering the XRD pattern aforementioned in Fig. 9, it can be inferred that a substance similar to the high temperature Zr—Si—O glass existed. Meanwhile, cracks induced by the volume shrinkage were formed during the cooling process.

Additionally, an apparent crack approximately 500 μm can be observed in the morphologies of the transition ablation region of ZS-0° as shown in Fig. 11(a). For clear observation, partial area in Fig. 11(a) was magnified into Fig. 11(b). Compared with Fig. 10(b), the fibers perpendicular to the flame as observed in the inset of Fig. 11(a) were located lower, and their cross-sections were flat or with pits. This region is deviated from the entrance. Therefore, less ZrB_2 and SiC were oxidized to generate a complete ZrO_2-SiO_2 layer as the temperature dropped. From another aspect, the reduced liquidity made this layer become hard to be blown away and the shear action of the gas flow also turned weak. So, the fibers below were protected from breakage. However, a molten phase that ZrO_2 particles pined in the continuous SiO_2 liquid glass was formed near the tail as observed in Fig. 11(b), from which it can be observed that the integral vertical cut slopes were of porous structures.

Fig. 11(c) shows the morphologies in most areas of the tail ablation region. It can be observed that a denser gray glassy SiO_2 layer was covered on the surface. According to the XRD patterns in aforementioned Fig. 9, more higher peaks of SiO_2 were detected at ZS-0°. When associated to the morphologies in Fig. 11(b), it could be deduced that a dual shield construction, in which a mixed oxide

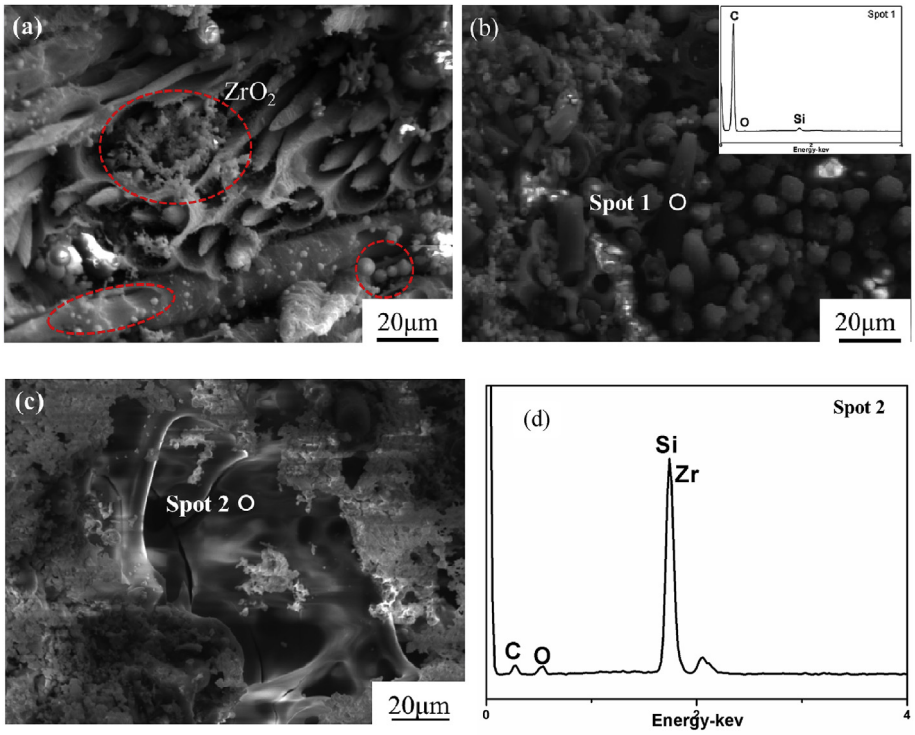

Fig. 10. Morphologies and relative EDS analysis of the entrance ablation region of ZS-0° sample after ablation: (a) sharp needle shapes; (b) flat-obtuse shapes with EDS inset; (c) molten state; (d) EDS curve.

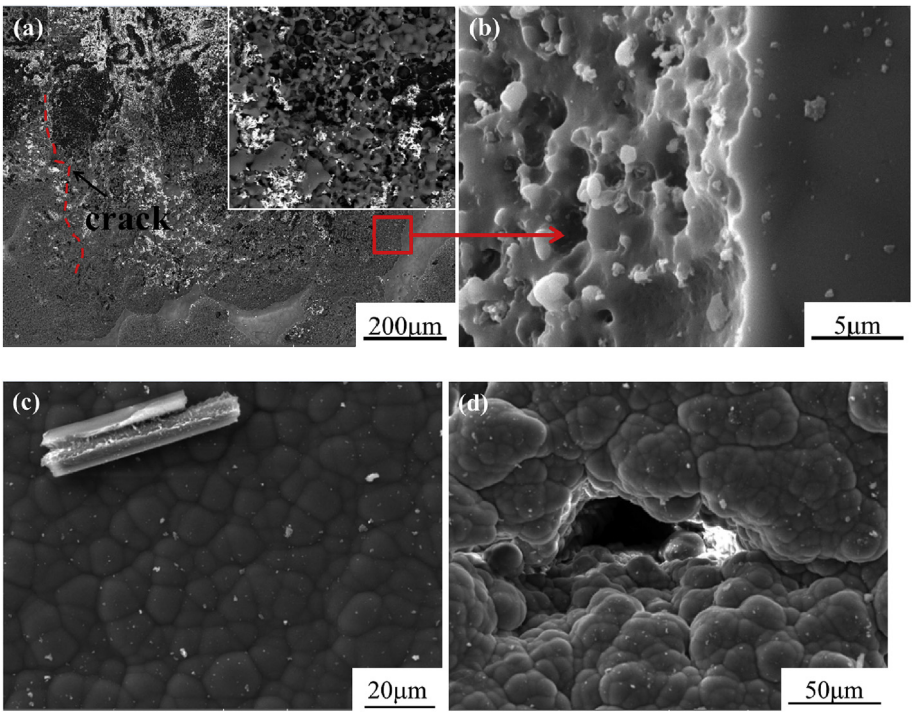

Fig. 11. Morphologies of the transition and the tail region of ZS-0° sample after ablation: (a) a crack in the surface as marked in red dash line; (b) magnification of partial area in (a) in which a gray white ZrO_2-SiO_2 sub-layer can be observed; (c) areas in the tail ablation region with scattered debris; (d) cave-like morphology with a relative large diameter in the tail region. (For interpretation of the references to color in this figure legend, the reader is referred to the Web version of this article.)

ZrO_2-SiO_2 sub-layer was under the upper protective SiO_2 layer, was formed in the tail region. However, there are some structural differences between this ZrO_2-SiO_2 sub-layer and the aforementioned holding-on ZrO_2-SiO_2 layer in ZS-90° as shown in aforementioned Fig. 8(e). It is believed that the ZrO_2-SiO_2 sub-layer rather than the holding-on phase plays the most important role in resisting ablation. This upper SiO_2 protective layer of ZS-0° was mostly derived from the surface of the entrance or the transition region. SiO_2 vapors in these regions can be blown away through the hole by the gas flow. Hence, with the reduction of the temperature and the gas flow washout, they will gradually attach onto the tail surface at a molten state, finally depositing into a dense SiO_2 layer. As a result, the size of the internal hole gradually decreased. These explanations are in good agreement with the diameter change curves of the internal hole shown in previous Fig. 7(a).

In addition, the fractured carbon fibers that split along the axis were also scoured away from other regions to the tail. Their debris were scattered on the upper SiO_2 layer as observed in Fig. 11(c). Some cave-like morphology with a relative large diameter can also be observed in the tail region as observed in Fig. 11(d), which is consistent with the macro-morphologies shown in previous Fig. 7(a). The reason is still under investigation now. However, the heat energy tended to be trapped in these holes and then accelerated the corrosion process in some way. It also indicated the existence of turbulent flame in the entrance hole. In a nutshell, that the ablation environment of ZS-0° samples experienced was severer than that of ZS-90°.

3.4. Ablation mechanism of the C/C-ZrB_2-SiC composites

Ablation is a fairly complicated process involving kinetics and thermodynamics [25,27]. Both ZS-90° and ZS-0° samples possess the identical phase compositions and almost the same Tmax, so they share roughly the same main reactions during the ablation process. Their ablation mechanisms included the physical and chemical reactions. The diverse morphologies analyzed previously signified that certain distinctions do exist between the ablation mechanisms of ZS-90° and ZS-0°. Fig. 12 shows the schematic diagram of the ablation mechanism of C/C-ZrB_2-SiC composites at different ablation angles. The corrosion is related to the temperature and the gas flow velocity of oxyacetylene flame. As mentioned above, the ablation lasts for 120 s and the Tmax of ZS-90° and ZS-0° rise to 2260 °C and 2300 °C, respectively. During ablation, following chemical reactions may possibly take place [10,13,14]:

$$C(s)+O_2(g)\rightarrow CO_n\,(g) \quad (4)$$

$$SiC(s)+\,O_2(g)\rightarrow SiO_2(l)+\,CO_n \quad (5)$$

$$SiC(s)+O_2(g)\rightarrow SiO(g)+CO_n\,(g) \quad (6)$$

$$SiO_2(l)+CO\,(g)\rightarrow SiO(g)+\,CO_2\,(g) \quad (7)$$

$$SiO_2(l)\rightarrow SiO_2(g) \quad (8)$$

$$2ZrB_2(s)+5O_2(g)\rightarrow ZrO_2(s)+B_2O_3(g) \quad (9)$$

$$ZrO_2(s)\rightarrow ZrO_2(l) \quad (10)$$

As to ZS-90°, the mass loss is mainly attributed to the oxidation of carbon matrix and fibers by Eq. (4). The oxidation of SiC is mainly determined by Eq. (5), and coupled with a small number of active oxidation of SiC in Eq. (6). It coincides with the formation of SiO_2 glass on the surface of Fig. 8(e). SiO_2 may also react with CO that was released by the oxidation in Eq. (7). While the gasification of SiO_2 in Eq. (8) also exists because the Tmax is 2260 °C. ZrB_2 has been oxidized into ZrO_2 and B_2O_3 by Eq. (9), and B_2O_3 (melting point 450 °C) didn't appear in the XRD pattern as a result of severe

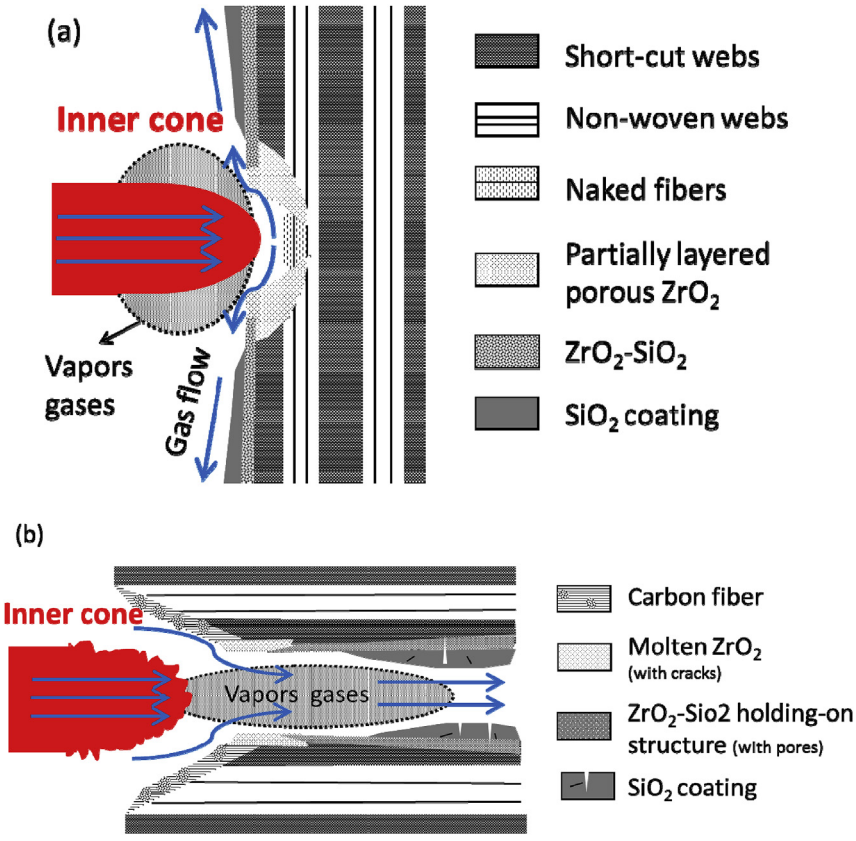

Fig. 12. Schematic diagram of the oxyacetylene ablation mechanism of C/C-ZrB_2-SiC composites at different ablation angles: (a) ablation schematic diagram of ZS-90°; (b) ablation schematic diagram of ZS-0°.

volatilization.

Based on the analysis above, an ablation schematic diagram of ZS-90° can be proposed as shown in Fig. 12(a), from which it can be inferred that the ablation is an interaction consequence of oxidation and thermo-mechanical denudation. The oxidation plays a major role and the thermo-mechanical denudation plays a minor role. The good ablation resistance can be explained from the following aspects:

First of all, ZrO_2 phase reacts with the little solute SiO_2, resulting in a lower melting point of ZrO_2 to form a molten structure expressed in Eq. (10). The molten ZrO_2 in Fig. 8(c) was not intact. It may provide an oxygen diffusion path so that the underlying composites can generate new oxides and provide ablation protection again. Secondly, the evaporation of B_2O_3 and SiO_2 can dissipate the heat in the composites and relax further ablation. Finally, the holding-on ZrO_2-SiO_2 layer and the dense upper SiO_2 layer can seal the solid grain boundaries and partly plug the ablation pores to prevent oxygen from permeating, which can offer excellent anti-ablation protection for the modified composites, only leading to a lower ablation mass.

The schematic diagram of ZS-0° is illustrated in Fig. 12(b). At this point, the crest of the turbulent flame that existed in the entrance hole is no longer smooth, but a jittery rough one. There is a gradient in the oxyacetylene flame, as the temperature of the inner cone is the highest and the outer envelope is the lowest [10]. According to the theory of Brownian movement, it can be known that higher temperature is accompanied by the faster surrounding gas molecule movement. In other words, the turbulent flame can create higher air velocity and severer gas scouring than laminar flame formed during the ablation of ZS-90°. Consequently, the ZrB_2-SiC multiple ceramics were oxidized more rapidly and peeled off easily. Meanwhile, SiO_2 was scoured away or evaporated through the hole. Carbon fibers and matrix were then exposed to an oxidizing atmosphere, being oxidized or fractured by mechanical breakage of the powerful shear force. Actually, the contact time between oxygen and fibers during the intense gas flow activities is short so that only very limited oxidative damage will generate. So, it can be concluded that the main destruction was caused by the mechanical denudation.

In conclusion, as a consequence of the formation of turbulent flame, peeling off of a large amount of molten ceramic oxides and fractured carbon fibers caused by the mechanical breakage finally generate a higher mass ablation rate than ZS-90°. In the transition and the tail ablation region, less ZrB_2 and SiC will be oxidized as the temperature and the air velocity can be further reduced. This upper protective SiO_2 layer in the tail region came mostly from the accumulation and deposition of the gaseous SiO_2 from other regions. As a result, an even smaller diameter of the internal hole than the original size (5 mm) and a negative linear ablation rate occurred in this region. According to the macroscopic and microscopic appearance analysis of ZS-0° after ablation, it can be drawn that the main destruction was caused by the mechanical denudation. The thermos-chemical ablation can serve as a supplementary failure mechanism.

4. Conclusions

The C/C-ZrB_2-SiC composites were prepared successfully via the precursor infiltration and pyrolysis method. When the prepared composites were ablated by oxyacetylene flame at 90° and

0° angles, respectively, for 120 s, the ZS-90° composites displayed excellent ablation resistance with the mass ablation rate of 2.075×10^{-4} g/s, whereas the mass ablation rate of the ZS-0° composites increased to 5.940×10^{-4} g/s. The liner ablation rate of ZS-90° sample is 1.3×10^{-3} mm/s, but for ZS-0° a negative liner ablation rate appears in the tail region.

By comparing the morphologies after ablation, it has been found that the ablation products on the surface of the composites may offer excellent ablation property for ZS-90°. Nevertheless, the layer of the ablation products in the internal hole of ZS-0° exhibits more visible defects which are undesired for ablation protection. The turbulent flame formed in the hole made a contribution to the poor ablation property.

When ZrB_2 and SiC were introduced into C/C composites, they were oxidized at high temperature to produce a protective ZrO_2 layer which protected the C/C composites from further ablation. The main destruction of the composites was caused by the mechanical denudation with the thermos-chemical ablation as a supplementary failure mechanism.

Acknowledgments

This work was financially supported by the Application Research of Creative Talents of Weinan Municipal Government under the Grant No.2017JCYJ-3-1 and by Shaanxi Province Engineering Laboratory of High Performance Concrete under the Grant No.G2016-03. It was also partially supported by the National Natural Science Foundation of China under Grant No.51472202 and No.5152106.

References

[1] Baosheng Xu, Yumin An, Peng Wang, Xinxin Jin, Guangdong Zhao, Microstructure and ablation behavior of double anti-oxidation protection for carbon-bonded carbon fiber composites, Ceram. Int. 43 (1) (2017) 783–790.
[2] Ke-Zhi Li, Tao Duan, Jia-Ping Zhang, Ning-Kun Liu, Mao-Yan Zhang, Ablation mechanism of carbon/carbon composites modified by HfC–SiC in two conditions under oxyacetylene torch, J. Mater. Sci. Technol. 33 (1) (2017) 71–78.
[3] Yujun Jia, Hejun Li, Qiangang Fu, Jiajia Sun, A ZrC-SiC/ZrC-LaB6/ZrC multilayer ablation resistance coating for SiC-coated carbon/carbon composites, Surface and Coatings Technology 309 (15) (2017) 545–553.
[4] Yang Liu, Jing-qiu Pei, Jiang Li, Guo-qiang He, Ablation characteristics of a 4D carbon/carbon composite under a high flux of combustion products with a high content of particulate alumina in a solid rocket motor, N. Carbon Mater. 32 (2) (2017) 143–150.
[5] Shameel Farhan, L.I. Ke-zhi, G.U.O. Ling-jun, G.A.O. Quan-ming, L.A.N. Feng-tao, Effect of density and fibre orientation on the ablation behaviour of carbon-carbon composites, N. Carbon Mater. 25 (3) (2010) 161–167.
[6] Junjie Ren, Kezhi Li, Shouyang Zhang, Xiyuan Yao, Song Tian, Preparation of carbon/carbon composite by pyrolysis of ethanol and methane, Mater. Des. 65 (2015) 174–178.
[7] Jie Ding, Zhixiong Huang, Yan Qin, Minxian Shi, Jiawei Mao, Improved ablation resistance of carbon–phenolic composites by introducing zirconium silicide particles, Compos. B Eng. 82 (12) (2015) 100–107.
[8] Ke-Zhi Li, Xue-Tao Shen, He-Jun Li, Shou-Yang Zhang, Lei-Lei Zhang, Ablation of the carbon/carbon composite nozzle-throats in a small solid rocket motor [J], Carbon 49 (4) (2011) 1208–1215.
[9] Yujun Jia, Hejun Li, Qiangang Fu, Jiajia Sun, Lu Li, Ablation behavior of ZrC-La2O3 coating for SiC-coated carbon/carbon composites under an oxyacetylene torch, Ceram. Int. 42 (12) (2016) 14236–14245.
[10] Cuiyan Li, Kezhi Li, Haibo Ouyang, Jianfeng Huang, Xingang Kong, Effect of ZrO2 morphology on the ablation resistance of carbon/carbon composites containing ZrC prepared by the carbothermal reduction reaction, Corrosion Sci. 102 (1) (2016) 405–412.
[11] Yue Liu, Qiangang Fu, Beibei Wang, Yiwen Guan, Yang Liu, Ablation behavior of C/C-SiC-ZrB2 composites in simulated solid rocket motor plumes, J. Alloys Compd. 727 (12) (2017) 135–145.
[12] L.I. Jun, Y.A.N.G. Xin, S.U. Zhe-an, X.U.E. Liang, L.I.U. Hong-wei, Effect of ZrC–SiC content on microstructure and ablation properties of C/C composites [J], Trans. Nonferrous Metals Soc. China 26 (10) (2016) 2653–2664.
[13] Zhenhua Hao, Wei Sun, Xiang Xiong, Yonglong Xu, Yalei Wang, Comparison of microstructure and ablation behavior of Si-Mo-Ti/Al/Zr infiltrated C/C composites prepared at different infiltration temperature, Ceram. Int. 43 (2) (2017) 2765–2773.
[14] Jalil Pourasad, Naser Ehsani, Zia Valefi, Sayed Ali Khalifesoltani, Preparation of a nanostructured SiC-ZrO2 coating to improve the oxidation resistance of graphite, Surf. Coating. Technol. 323 (8) (2017) 58–64.
[15] F.U. Qian-gang, Z.H.A.N.G. Jia-ping, Z.H.A.N.G. Zheng-zhong, L.I. He-jun, S.U.N. Can, SiC–MoSi2/ZrO2–MoSi2 coating to protect C/C composites against oxidation, Trans. Nonferrous Metals Soc. China 23 (7) (2013) 2113–2117.
[16] Yulei Zhang, Heng Hu, Pengfei Zhang, Zhixiong Hu, Leilei Zhang, SiC/ZrB2–SiC–ZrC multilayer coating for carbon/carbon composites against ablation, Surf. Coating. Technol. 300 (8) (2016) 1–9.
[17] Xiaochao Jin, Xueling Fan, Chunsheng Lu, Tiejun Wang, Advances in oxidation and ablation resistance of high and ultra-high temperature ceramics modified or coated carbon/carbon composites, J. Eur. Ceram. Soc. 38 (1) (2018) 1–28.
[18] Tao Feng, He-Jun Li, Man-Hong Hu, Hong-Jiao Lin, Lu Li, Oxidation and ablation resistance of Fe2O3 modified ZrB2-SiC-Si coating for carbon/carbon composites, Ceram. Int. 42 (1) (2016) 270–278.
[19] Peipei Wang, Hejun Li, Yujun Jia, Yulei Zhang, Ruimei Yuan, Ablation resistance of HfB2-SiC coating prepared by in-situ reaction method for SiC coated C/C composites[J], Ceram. Int. 43 (15) (2017) 12005–12012.
[20] Dini Wang, Yi Zeng, Xiang Xiong, Guodong Li, Yalei Wang, Preparation and ablation properties of ZrB2-SiC protective laminae for carbon/carbon composites, Ceram. Int. 40 (9) (2014) 14215–14222.
[21] Lei Zhuang, Qian-Gang Fu, He-Jun Li, SiCnw/PyC core-shell networks to improve the bonding strength and oxyacetylene ablation resistance of ZrB2-ZrC coating for C/C-ZrB2-ZrC-SiC composites, Carbon 124 (11) (2017) 675–684.
[22] Baosheng Xu, Rujie He, Changqing Hong, Yongbin Ma, Yazheng Yang, Ablation behavior and mechanism of double-layer ZrB2-based ceramic coating for lightweight carbon-bonded carbon fiber composites under oxyacetylene flame at elevate temperature, J. Alloys Compd. 702 (4) (2017) 551–560.
[23] Mao-yan Zhang, Ke-zhi Li, Xiao-hong Shi, Wen-long Tan, Effects of SiC interphase on the mechanical and ablation properties of C/C-ZrC-ZrB2-SiC composites prepared by precursor infiltration and pyrolysis, Mater. Des. 122 (5) (2017) 322–329.
[24] Jinhua Lu, Kui Hao, Lei Liu, Hejun Li, Xin Yan, Ablation resistance of SiC–HfC–ZrC multiphase modified carbon/carbon composites, Corrosion Sci. 103 (2) (2016) 1–9.
[25] L.K. Su, O.S. Sun, M.G. Mungal, Experimental investigation of stabilization mechanisms in turbulent, lifted jet diffusion flames, Combust. Flame 144 (3) (2006) 494–512.
[26] C. Pradere, C. Sauder, Transverse and longitudinal coefficient of thermal expansion of carbon fibers at high temperatures (300-2500K), Carbon 46 (14) (2008) 1874–1884.
[27] Mir Asad Mirzapour, Hasan Rezaei Haghighat, Zahra Eslami, Effect of zirconia on ablation mechanism of asbestos fiber/phenolic composites in oxyacetylene torch environment, Ceram. Int. 39 (8) (2013) 9263–9272.